UNIVERSITY OF LEEDS

This is a repository copy of *Phase-reduction analysis of periodic thermoacoustic oscillations in a Rijke tube*.

White Rose Research Online URL for this paper:
https://eprints.whiterose.ac.uk/181924/

Version: Accepted Version

Article:

Skene, CS orcid.org/0000-0003-0994-2013 and Taira, K (2022) Phase-reduction analysis of periodic thermoacoustic oscillations in a Rijke tube. Journal of Fluid Mechanics, 933. A35. ISSN 0022-1120

https://doi.org/10.1017/jfm.2021.1093

© The Author(s), 2021. Published by Cambridge University Press. "This article has been published in a revised form in Journal of Fluid Mechanics https://doi.org/10.1017/jfm.2021.1093. This version is free to view and download for private research and study only. Not for re-distribution, re-sale or use in derivative works.

Reuse

This article is distributed under the terms of the Creative Commons Attribution-NonCommercial-NoDerivs (CC BY-NC-ND) licence. This licence only allows you to download this work and share it with others as long as you credit the authors, but you can’t change the article in any way or use it commercially. More information and the full terms of the licence here: https://creativecommons.org/licenses/

Takedown

If you consider content in White Rose Research Online to be in breach of UK law, please notify us by emailing eprints@whiterose.ac.uk including the URL of the record and the reason for the withdrawal request.

White Rose university consortium
Universities of Leeds, Sheffield & York

eprints@whiterose.ac.uk
https://eprints.whiterose.ac.uk/

Banner appropriate to article type will appear here in typeset article

Phase reduction analysis of periodic thermoacoustic oscillations in a Rijke tube

Calum S. Skene[1]†‡ and Kunihiko Taira[1]

[1]Department of Mechanical and Aerospace Engineering, University of California, Los Angeles, CA 90095, USA

(Received xx; revised xx; accepted xx)

Phase reduction analysis captures the linear phase dynamics with respect to a limit cycle subjected to weak external forcing. We apply this technique to study the phase dynamics of the self-sustained oscillations produced by a Rijke tube undergoing thermoacoustic instability. Through the phase reduction formulation, we are able to reduce these dynamics to a scalar equation for the phase, allowing us to efficiently determine the synchronisation properties of the system. For the thermoacoustic system, we find the conditions for which $m : n$ frequency locking occurs, shedding light on the mechanisms behind asynchronous and synchronous quenching. We also reveal the optimal placement of pressure actuators that provide the most efficient route to synchronisation.

Key words:

1. Introduction

Due to heightened environmental regulations, there has been a move towards using lean premixed combustors (LPCs) for their ability to operate at lower temperatures in a low $\mathsf{NO_x}$ regime (Correa 1998). Whilst there are many health and environmental advantages to avoiding the production of $\mathsf{NO_x}$, which is a lung irritant and can cause acid rain and depletion of the Ozone layer (Mahashabde *et al.* 2011), LPCs present many practical issues, including their susceptibility towards thermoacoustic instability (Culick 1996; Lieuwen & Yang 2005).

Thermoacoustic instability arises due to a feedback mechanism between acoustic waves and unsteady heat release. Unsteady heat release produces acoustic fluctuations which in turn interact with the flame causing more unsteady heat release. If these acoustic fluctuations are in phase with the unsteady heat release, this causes energy to be added to the system, which can lead to instability. This mechanism was first described by Rayleigh, J. L. (1878) who summarised it by

† Email address for correspondence: c.s.skene@leeds.ac.uk
‡ Present address: Department of Applied Mathematics, University of Leeds, Leeds LS2 9JT, UK

Abstract must not spill onto p.2

a simple, but effective, integral criterion. Even though Rayleigh's criterion for instability is mathematically simple, the fact that this mechanism is extremely sensitive to the parameters of the system (Juniper & Sujith 2018) means that the accurate prediction of thermoacoustic instabilities is a difficult task, leading to many combustion systems being built vulnerable to these instabilities.

As these instabilities can cause material fatigue and lifetime reduction for these systems, it is critical to develop control strategies to either suppress, or remove entirely, these instabilities (Candel 2002). These control strategies can fall into two categories: active (McManus *et al.* 1993; Zhao *et al.* 2018) and passive (Zhao & Li 2015). Examples of passive control include the addition of Helmholtz resonators to provide acoustic damping (Dupère & Dowling 2005). On the other hand, active control uses actuation devices such as loudspeakers to provide an additional source of acoustic waves (Dowling & Morgans 2005). Furthermore, the aforementioned sensitivity of these systems to parameters has made adjoint methods an attractive tool in designing these controls (Magri 2019), for example in optimising the shape and placement of Helmholtz resonators (Yang *et al.* 2019) or for discovering the optimal feedback mechanism for suppressing the growth rate of instabilities (Magri & Juniper 2013). Of particular relevance to our study is open-loop control via harmonic forcing of the thermoacoustic system and adjoint design methods based on Floquet theory (Magri 2019).

By introducing harmonic forcing, the phase relationship between the unsteady heat release and pressure perturbations can be disrupted leading to a decrease in the self-sustained limit cycle oscillations (Kashinath *et al.* 2018; Mondal *et al.* 2019; Roy *et al.* 2020). Depending on the value of the forcing frequency in relation to the natural frequency of the limit cycle, this decrease can be split into two cases. Synchronous quenching occurs if the forcing is close to the natural frequency and although the self-excited oscillations are suppressed, the system synchronises to the forcing frequency, causing a resonant amplification. On the other hand, if the forcing frequency is farther away from the natural frequency, then a reduction in the self-excited oscillations can occur without resonant amplification. Therefore, understanding a-priori the synchronisation properties of the system is of upmost importance in order to determine good candidate frequencies, and forcing shapes, that result in synchronisation away from resonant frequencies. The aim of this study is to apply phase reduction analysis to thermoacoustic systems, an adjoint-Floquet-based method, which will allow the synchronisation characteristics of the system to be obtained efficiently from numerical simulations. Furthermore, we will showcase the usefulness of this information in the design of open-loop control strategies via harmonic forcing.

Phase reduction analysis is a technique that has been widely used for studying the dynamics of synchronisation in biological systems (Kuramoto 1984; Pikovsky *et al.* 2003; Ermentrout & Terman 2010; Boccaletti *et al.* 2018). It is only relatively recently that phase reduction been introduced to the fluids community (Kawamura & Nakao 2015; Taira & Nakao 2018; Iima 2019; Khodkar & Taira 2020; Nair *et al.* 2021; Khodkar *et al.* 2021; Loe *et al.* 2021). In essence, phase reduction allows the linear phase dynamics of a stable periodic system to be represented by a simple scalar ordinary differential equation (ODE) for the phase. This ODE is characterised by the phase sensitivity function which encodes properties of how external forcing affects the phase. Obtaining the phase sensitivity function therefore allows for the efficient determination of the synchronisation properties of the underlying system, which in the present study is focused on thermoacoustic

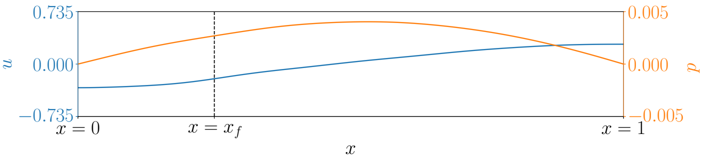

Figure 1: Rijke tube setup with example velocity and pressure profiles.

systems. In what follows, section 2 outlines the Rijke tube model, section 3 lays out the mathematics of phase reduction analysis, the numerics are described in section 4, the results are presented in section 5 and finally, the conclusions are offered in section 6. Appendix A contains further mathematical details of the method, as well as solidifying the link between phase sensitivity analysis and Floquet theory (Floquet 1883) for delay differential equations (Simmendinger *et al.* 1999).

2. The Rijke tube: An example thermoacoustic system

A Rijke tube (Rijke 1859) is a relatively simple setup that exhibits a rich range of dynamics with thermoacoustic instability. We show the basic setup in figure 1 and model the system as a one-dimensional flow in a pipe. The left side of the pipe is aligned with $x = 0$, with the pipe having a non-dimensional unit length. A heat source is placed at $x = x_f$, and is modeled as a thin wire using a modified version (Heckl 1990) of Kings law (King 1914).

Following the derivation in Sayadi *et al.* (2014), the non-dimensional governing equations for this system is provided by

$$\frac{\partial u}{\partial t} + (\gamma Ma)^{-1}\frac{\partial p}{\partial x} = 0, \tag{2.1}$$

$$\frac{\partial p}{\partial t} + (\gamma Ma)\frac{\partial u}{\partial x} + \xi * p = \gamma Ma Q + \epsilon f_p^+, \tag{2.2}$$

for the velocity u and the pressure p, which form our state space $\boldsymbol{y} = (u, p)^T$. Following the work of Mondal *et al.* (2019), a weak external pressure forcing f_p^+ with amplitude $\epsilon \ll 1$ is added to the pressure field. The governing equations hold two non-dimensional parameters of Mach number Ma and the specific heat ratio γ. The damping for wavenumber j is given via a convolution $*$ in terms of damping coefficients c_1 and c_2 as $\xi_j = c_1 j^2 + c_2\sqrt{j}$. We see that the only nonlinearity that enters the equation is through the heat release rate term,

$$Q = Q_f(t-\tau)\delta(x - x_f) = \frac{K}{2}\left[\sqrt{|1/3 + u_f(t-\tau)|} - \sqrt{1/3}\right]\delta(x - x_f), \tag{2.3}$$

which is localised to the flame location x_f, using a Dirac delta function δ, with a time-dependent amplitude Q_f that depends on the velocity at the flame u_f, flame time delay τ and the heater strength K. This system is a delay partial differential equation (DPDE) due to the lag introduced through the heating term. Therefore, the initial condition for this equation must be specified for $t \in [t_0 - \tau, t_0]$. We apply open boundaries at the pipe ends, which correspond to homogeneous Dirichlet and Neumann conditions for p and u, respectively.

For a sufficiently large K, the fixed point $(u, p) = (0, 0)$ is unstable and, for all parameters regimes considered in this study, non-linear saturation of this instability yields a self-sustained limit cycle with period T. As we are dealing with a DPDE whose solution must be known over $[t-\tau, t]$ in order to propagate the solution forward, the limit cycle is actually defined up to τ time-units previously. To make this dependence on the history of the system clear, we now introduce the following notation (Hale 1977) (see appendix A for further details). In what follows, we consider the discretised system and write the state-equation as the delay differential equation (DDE)

$$\dot{\boldsymbol{y}} = \boldsymbol{f}(t, \boldsymbol{y}(t)) + \boldsymbol{g}(t-\tau, \boldsymbol{y}(t-\tau)) + \epsilon \boldsymbol{h}(t), \tag{2.4}$$

with $\boldsymbol{f}$, $\boldsymbol{g}$ and $\boldsymbol{h}$ arising from the discretisation of (2.2). We write a solution to this equation in the form $\boldsymbol{y}_t(\phi) = \boldsymbol{y}(t+\phi)$ where $\phi \in [-\tau, 0]$. In particular, we can express our limit cycle, a periodic solution in the absence of forcing ($\epsilon = 0$), as $\boldsymbol{y}_t^{\mathrm{LC}}(\phi)$, where $\boldsymbol{y}_{t+T}^{\mathrm{LC}}(\phi) = \boldsymbol{y}_t^{\mathrm{LC}}(\phi)$.

3. Phase reduction analysis

For a given limit cycle, we can introduce the concept of phase through a two-part definition. First, we associate the phase θ with states $\boldsymbol{y}_t^{\mathrm{LC}}(\phi)$ on the limit cycle via $\theta = 2\pi t/T \bmod 2\pi$. Hence, the phase $\theta \in [0, 2\pi]$ is a scalar variable that represents the limit cycle. Second, we extend the phase definition to states in the vicinity of our limit cycle by restricting ourselves to limit cycles that are asymptotically stable. This means that if $\boldsymbol{y}_t(\phi)$ is a state not necessarily on the limit cycle then there exists a state on the limit cycle $\boldsymbol{y}_{t+\alpha}^{\mathrm{LC}}(\phi)$ such that $\|\boldsymbol{y}_t(\phi) - \boldsymbol{y}_{t+\alpha}^{\mathrm{LC}}(\phi))\| \to 0$ as $t \to \infty$. We can then say that the phase of $\boldsymbol{y}_t(\phi)$ is the same as the point in time it asymptotically tends to and therefore $\Theta(\boldsymbol{y}_t(\phi)) = \Theta(\boldsymbol{y}_{t+\alpha}^{\mathrm{LC}}(\phi))$ where the phase function Θ is defined such that $\Theta(\boldsymbol{y}_t(\phi)) = \theta$. While the phase is directly related to the time variable in this problem, phase can in general be related to sensor measurements (Taira & Nakao 2018). It is also worth noting that whilst alternative definitions of phase can be introduced, the motivation behind our definition is that it will allow us to study the synchronisation properties of the limit cycle using linear theory.

For states on the limit cycle the phase θ satisfies $\dot{\theta} = \omega_n = 2\pi/T$ where ω_n is the angular frequency of the limit cycle. However, in the presence of a small external forcing, the phase equation becomes (Kotani *et al.* 2012; Novičenko & Pyragas 2012)

$$\dot{\theta} = \omega_n + \epsilon \boldsymbol{Z}(\theta)^T \boldsymbol{h}(t) + \mathcal{O}(\epsilon^2). \tag{3.1}$$

The function $\boldsymbol{Z}(\theta)$ is the phase-sensitivity function, and allows us to assess the influence of a perturbation $\boldsymbol{h}(t)$ on the phase-dynamics. In order to determine this phase sensitivity function, two main methods can be employed. The first of which is to perturb the equation for a range of values of θ, building up the function one point at a time (Taira & Nakao 2018). A second approach, which we consider, finds $\boldsymbol{Z}$ as the solution to an adjoint problem (Kotani *et al.* 2012; Novičenko & Pyragas 2012).

For the latter approach, we begin by linearising the unperturbed governing equations (2.4) about the limit cycle $\boldsymbol{y}_t^{\mathrm{LC}}(\phi)$ providing the linear DDE

$$\dot{\boldsymbol{y}}' = \boldsymbol{A}_1(t)\boldsymbol{y}'(t) + \boldsymbol{A}_2(t)\boldsymbol{y}'(t-\tau). \tag{3.2}$$

This equation describes the dynamics of a small perturbation $\boldsymbol{y}'$ about the limit cycle. Here, the matrices $\boldsymbol{A}_1$ and $\boldsymbol{A}_2$ are the Jacobians $\boldsymbol{A}_1(t) = \nabla_{\boldsymbol{y}} \boldsymbol{f}(\boldsymbol{y})|_{\boldsymbol{y}=\boldsymbol{y}_t(0)}$ and

Focus on Fluids articles must not exceed this page length

$\boldsymbol{A}_2(t) = \nabla_{\boldsymbol{y}} \boldsymbol{g}(\boldsymbol{y})|_{\boldsymbol{y}=\boldsymbol{y}_t(-\tau)}$, respectively.As discussed more extensively in appendix A, we must first define a bilinear form to introduce the adjoint for a DDE. For the present DDE, the appropriate bilinear form (Kotani *et al.* 2012; Novičenko & Pyragas 2012) is

$$\langle \boldsymbol{a}(t), \boldsymbol{b}(t) \rangle \equiv \boldsymbol{a}(t)^T \boldsymbol{b}(t) + \int_{-\tau}^{0} \boldsymbol{a}(t+\tau+\xi)^T \boldsymbol{A}_2(t+\tau+\xi) \boldsymbol{b}(t+\xi)\, \mathrm{d}\xi. \tag{3.3}$$

Using this bilinear form, the adjoint can be found (see appendix A) to satisfy the adjoint equation

$$\dot{\boldsymbol{y}}^\dagger = -\boldsymbol{A}_1^T(t) \boldsymbol{y}^\dagger(t) - \boldsymbol{A}_2^T(t+\tau) \boldsymbol{y}^\dagger(t+\tau). \tag{3.4}$$

With the linear equation (3.2) and its adjoint (3.4), we can find the phase sensitivity function via the link between a phase shift and Floquet theory, which governs the stability of the limit cycle. As we have assumed that the limit cycle is stable, all the Floquet exponents are inside the unit circle, except for one which provides the phase shift. Indeed, for an autonomous system there is always one neutral Floquet exponent which has the eigenvector $\dot{\boldsymbol{y}}_t^{\mathrm{LC}}(\phi)$.

The Floquet exponents for the adjoint system (3.4) are the negative complex conjugates of the direct case. This means that by solving equation (3.4) backwards in time, the system is stable and has one neutral Floquet exponent with the corresponding eigenvector $\boldsymbol{y}_t^\dagger(\phi)$. Normalising this eigenvector such that $\langle \boldsymbol{y}_t^\dagger(\phi), \dot{\boldsymbol{y}}_t^{\mathrm{LC}}(\phi) \rangle = \omega_n$ yields the phase sensitivity function via $\boldsymbol{Z}(\theta) = \boldsymbol{y}^\dagger_{t=\theta/\omega_n}(0)$ (see appendix A for details). In practice, we can find the adjoint eigenvector by integrating equation (3.4) back in time from an arbitrary initial condition to obtain the 'adjoint limit-cycle,' which given a sufficiently long time horizon converges to the neutral Floquet solution.

Using the phase sensitivity function, the phase coupling function can be determined. We consider the general case of $m:n$ phase locking, meaning that for m periods of the external forcing, the system completes n cycles. By introducing the phase difference $\Delta\theta(t) = \theta(t) - (n/m)\omega_f t$, and assuming that $\Delta\theta(t)$ is slowly varying, it can be shown (see Khodkar & Taira (2020) for example) that synchronisation will occur if

$$\epsilon \min_{\Delta\theta} \Gamma_{m,n}(\Delta\theta) < (n/m)\omega_f - \omega_n < \epsilon \max_{\Delta\theta} \Gamma_{m,n}(\Delta\theta), \tag{3.5}$$

where

$$\Gamma_{m,n}(\Delta\theta) \equiv \frac{1}{mT_f} \int_{t_0}^{t_0+mT_f} \boldsymbol{Z}\left(\Delta\theta(t) + (n/m)\omega_f s\right)^T \boldsymbol{h}(s) \mathrm{d}s, \tag{3.6}$$

is the phase coupling function and T_f is the period of the external forcing. This inequality gives a region of synchronisation over the space of forcing angular frequency ω_f and forcing amplitude ϵ, known as an Arnold tongue, in which $m:n$ frequency locking is possible.

4. Numerical implementation

To numerically solve the governing equations (2.2), we consider the Galerkin projection approach of Balasubramanian & Sujith (2008). With expansions

$$u = \sum_{j=1}^{N} \eta_j(t) \cos(j\pi x), \tag{4.1}$$

$$p = -\sum_{j=1}^{N} \left(\frac{\dot{\eta}_j(t)\gamma Ma}{j\pi} \right) \sin(j\pi x), \tag{4.2}$$

$$f_p^+ = \sum_{j=1}^{N} f_{pj}^+ \sin(j\pi x), \tag{4.3}$$

we automatically satisfy the boundary conditions and reduce the full DPDE to a DDE for the coefficients η_j and $\dot{\eta}_j$. The heat release terms become

$$u_f = \sum_{j=1}^{N} \eta_j(t-\tau) \cos(j\pi x_f), \tag{4.4}$$

$$\dot{q}_j = j\pi K \left(\sqrt{|1/3 + u_f|} - \sqrt{1/3} \right) \sin(j\pi x_f), \tag{4.5}$$

and we can write the system (2.2) as

$$\ddot{\eta}_j + (j\pi)^2 \eta_j + \xi_j \dot{\eta}_j = -\dot{q}_j - \frac{j\pi\epsilon}{\gamma Ma} f_{pj}^+. \tag{4.6}$$

This equation can be recast to the first order DDE

$$\frac{\mathrm{d}}{\mathrm{d}t} \begin{pmatrix} \boldsymbol{\eta}(t) \\ \dot{\boldsymbol{\eta}}(t) \end{pmatrix} = \begin{pmatrix} \boldsymbol{0} & \boldsymbol{I} \\ \boldsymbol{W} & \boldsymbol{D} \end{pmatrix} \begin{pmatrix} \boldsymbol{\eta}(t) \\ \dot{\boldsymbol{\eta}}(t) \end{pmatrix} - \begin{pmatrix} \boldsymbol{0} \\ \dot{\boldsymbol{q}}(\boldsymbol{\eta}(\boldsymbol{t}-\boldsymbol{\tau})) \end{pmatrix} - \epsilon \begin{pmatrix} \boldsymbol{0} \\ \boldsymbol{f}_p^+ \end{pmatrix}, \tag{4.7}$$

where

$$\boldsymbol{\eta} = (\eta_1, ..., \eta_N)^T, \quad \boldsymbol{f}_p = (\pi/(\gamma Ma) f_{p1} ..., N\pi/(\gamma Ma) f_{pN})^T \tag{4.8}$$

and diagonal matrices $\boldsymbol{W}$ and $\boldsymbol{D}$ have entries $\boldsymbol{W}_{jj} = -(j\pi)^2$ and $\boldsymbol{D}_{jj} = -\xi_j$, respectively.

It is important to note that the size of ϵ does not affect the phase sensitivity function $\boldsymbol{Z}$ as this is determined through a linear formulation. However, when the phase sensitivity function is used to find the bounds of synchronisation via equation (3.5), we are in effect using a first-order Taylor expansion in ϵ in which $\boldsymbol{Z}$ is the linear term. Therefore, the size of ϵ can affect the synchronisation region. Indeed, ϵ is the amplitude of the external forcing, and it is useful to have a physical measure of how large this amplitude is. To this end, we introduce the total non-dimensional acoustic energy per unit volume of the system (Juniper 2011)

$$E = \frac{1}{2}\left[u^2 + \frac{p^2}{(\gamma Ma)^2} \right] = \frac{1}{2}\sum_{j=1}^{N} \eta_j^2 + \frac{1}{2}\sum_{j=1}^{N} \left(\frac{\dot{\eta}_j}{j\pi} \right)^2. \tag{4.9}$$

This energy measure allows us to quantify the size of ϵ. In other words, we assess the magnitude of the added perturbation.

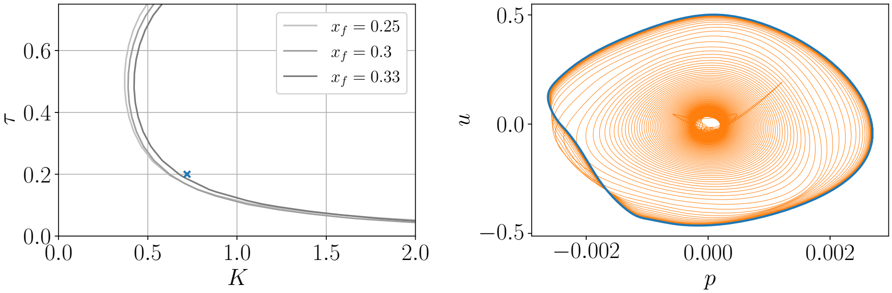

Figure 2: (left) Neutral curves for the stability of the fixed point $(u, p) = (0, 0)$. Highlighted with a blue cross are the parameters for our base case. (right) Plot of u against p at $x = 0.2$ for the direct solution. The transient behaviour is displayed in orange, with the limit cycle shown in blue.

To obtain the linearised and adjoint equations, we cast the Galerkin model (4.7) in the form of a DDE (2.4). Here, we have

$$\boldsymbol{A}_1 = \begin{pmatrix} \boldsymbol{0} & \boldsymbol{I} \\ \boldsymbol{W} & \boldsymbol{D} \end{pmatrix}, \qquad \boldsymbol{A}_2 = \begin{pmatrix} \boldsymbol{0} & \boldsymbol{0} \\ \boldsymbol{B} & \boldsymbol{0} \end{pmatrix}, \tag{4.10}$$

in our linearised equation (3.2) where

$$(\boldsymbol{B})_{ij}(t) = -\frac{i\pi K \sin(i\pi x_f)\operatorname{sgn}(\frac{1}{3} + u_f(t-\tau))\cos(j\pi x_f)}{2\sqrt{\left|\frac{1}{3} + u_f(t-\tau)\right|}}. \tag{4.11}$$

Our implementation, which is available (Skene & Taira 2021), is based on the sixth order DDE solver *Vern6* (Verner 2010) contained in the *DifferentialEquations.jl* package (Rackauckas & Nie 2017).

5. Results

Using the Galerkin expansion approach introduced above, we are able to systematically obtain the phase sensitivity function for a given set of parameters. As our goal is not only to find the phase sensitivity function, but also to assess the synchronisation dynamics with a view to open-loop forcing, we consider a range of values for the flame time delay τ, flame strength K and flame location x_f. For all cases, we fix the number of Galerkin modes to $N = 10$, which gives a reasonable compromise between obtaining higher-mode behaviour and keeping the computational run-time reasonable. We herein set the damping parameters to $c_1 = 0.1$ and $c_2 = 0.06$ and fix $Ma = 0.005$ and $\gamma = 1.4$. The neutral stability curves for the fixed point $(u, p) = (0, 0)$ in $\tau - K$ space for different values of the flame location are shown in figure 2 (left). In what follows, we only consider unstable cases as this will ensure that a limit cycle solution emerges. However, even in the stable regime, limit cycle solutions can be found, as in the study by Juniper (2011) and the methods of this paper also carry over to these limit cycles, provided they are Floquet stable. It is also worth noting that Juniper (2011) showed that due to non-normality a small perturbation can grow large enough to move the system away from its stable configuration, an effect which is not accounted for by our current analysis which is valid close to the limit cycle.

We start by examining the case with $K = 0.72$, $x_f = 0.25$ and $\tau = 0.2$,

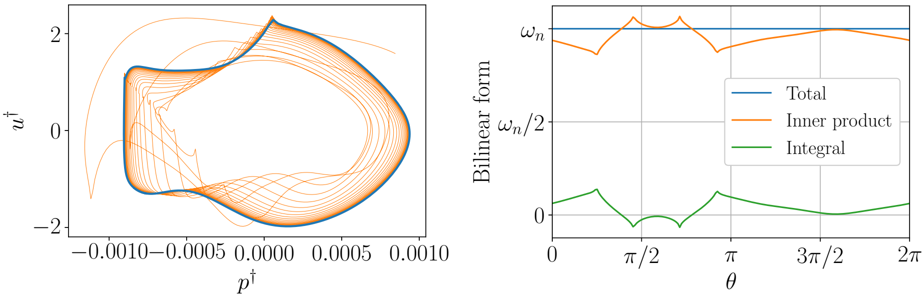

Figure 3: (left) Plot of $u^\dagger$ against $p^\dagger$ at $x = 0.2$ for adjoint solution. Again, the transient behaviour is displayed in orange, with the limit cycle shown in blue. (right) The value of the bilinear form, as well as the breakdown into its inner product and integral contributions, over one period.

following Mondal *et al.* (2019). This baseline case is highlighted in figure 2 (left) and is located just inside the unstable regime. To obtain the limit cycle, we solve equation (4.7) in the absence of external forcing and with a small random initial condition. For these parameters, the state $(u, p) = (0, 0)$ is unstable, the perturbation grows, and eventually saturates into a limit cycle. By starting at $t = -400$, we obtain a limit cycle (see figure 2 (right)) free of transient effects by $t = 0$, which is further integrated to $t = 400$. This allows us to obtain the phase sensitivity function by solving the adjoint equation backwards in time, starting from a random initial condition, from $t = 400$ to 0 (see figure 3 (left)). We compute the phase sensitivity function using the adjoint solution for $t \in [0, T]$ with $T = 1.93$, scaling with the normalisation specified in section 3. Whilst enabling us to fix the amplitude of the phase sensitivity function, the inner product (3.3) also provides a good check of our adjoint solution. The inner product must be constant in time and consists of two parts; a dot product and an integral. Figure 3 (right) confirms the value the inner product being constant over one period, verifying our adjoint solution.

With the phase sensitivity function determined, we can compute the phase coupling function using equation (3.6). The forcing term is specified to be $f^+_{pj} = -\gamma Ma/(j\pi)c\cos(\omega_f t)$ following Mondal *et al.* (2019), with c chosen such that the forcing has a unit acoustic energy norm. The resulting Arnold tongue obtained from criteria (3.5) is shown in figure 4 (left). We have shown on the y-axis both the amplitude ϵ as well as A_f which matches the amplitude displayed by Mondal *et al.* (2019) due to the different normalisations used. The 'V' shape shows the minimum amplitude of the forcing needed to obtain synchronisation at the different values of the frequency $f = \omega_f/(2\pi)$, with synchronisation being possible inside the V-shaped region. We see that for frequencies equal to the natural frequency of the system f_n, synchronisation is always possible. However, as this frequency is increased or decreased a greater forcing amplitude is needed.

Figure 4 (left) shows that there is a good agreement with our obtained Arnold tongue and the one computed by Mondal *et al.* (2019) which holds true even for large forcing amplitudes ϵ. The Arnold tongue calculated by Mondal *et al.* (2019) required performing a series of nonlinear simulations at different forcing amplitudes to obtain, on a point-by-point basis, the resulting synchronisation behaviour. This means that the Arnold tongue they obtain includes nonlinear behaviour, such as phase trapping. In our case, we consider a linear analysis

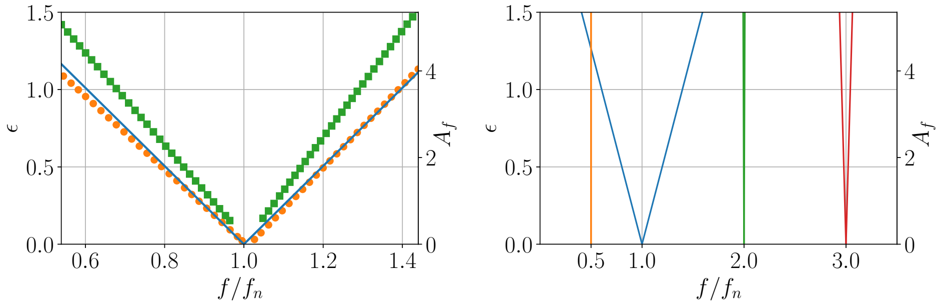

Figure 4: (left) The Arnold tongue showing the regions where synchronisation is possible (blue line). Also displayed are the boundaries between phase trapping and phase drifting (orange circles), as well as phase locking and phase trapping (green squares) from Mondal *et al.* (2019). (right) The Arnold tongues for the general cases of 1 : 2 (orange), 1 : 1 (blue), 2 : 1 (green) and 3 : 1 (red) synchronisation.

which enables us to efficiently calculate the entire Arnold tongue with a single adjoint simulation. The differences can be therefore be attributed to non-linear effects. We also see that our Arnold tongue is symmetric. This symmetry has to occur when using a Galerkin model since both u and p have zero means. However, the experimentally obtained Arnold tongue (Mondal *et al.* 2019) has an asymmetry showing that synchronisation was easier for frequencies below the natural frequency. This is a direct consequence of their experimental setup which has a mean flow.

In addition to 1 : 1 synchronisation, figure 4 (right) reveals the general case of $m : n$ phase locking predicted by the present analysis. The figure shows that 1 : 1 synchronisation is the easiest to achieve, with 3 : 1 frequency locking also being feasible, albeit over a narrower region. Perhaps most importantly, we see that for our system 1 : 2 synchronisation is impractical to attain. In the study of Mondal *et al.* (2019), asynchronous quenching was achieved for frequencies lower than the natural frequency, a region in which 1 : 2 type phase locking could occur. By obtaining figure 4 (right), we can directly observe a-priori the phase locking behaviour in this region. This further emphasises the importance of obtaining the Arnold tongues in designing open-loop control strategies, and highlights the capabilities of the phase sensitivity method to efficiently find the synchronisation conditions.

The fact that the phase sensitivity function is independent of the forcing function means that we can efficiently consider the optimal placement of the pressure forcing for the purpose of synchronisation. Identifying the optimal placement allows for designing effective open-loop control strategies to move the frequency of the limit cycle to a desired one for a particular system via synchronisation. This is similar to the approach of Khodkar & Taira (2020), where the optimal placement of actuators for synchronisation was considered in the case of vortex shedding behind a cylinder. To assess the ease (or difficulty) of achieving synchronisation, we consider synchronisability $\mathcal{S} \equiv \max(\mathit{\Gamma}) - \min(\mathit{\Gamma})$, which essentially represents the width of the the Arnold tongue (Khodkar & Taira 2020). Instead of a global pressure forcing, we now consider a pointwise placement of pressure actuation given by $f_p^+ = \gamma Ma\delta(x - x_p)\cos(\omega_f t)$, where x_p is the actuator location along the Rijke tube. In terms of our Galerkin model, this corresponds to setting

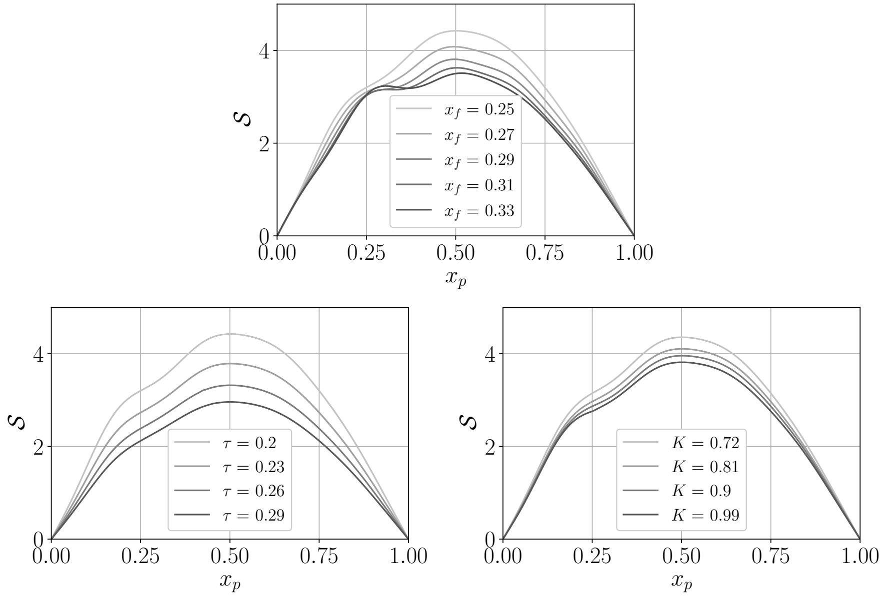

Figure 5: The synchronisability as the pressure actuation location is varied along the tube. (top) $K = 0.72$, $\tau = 0.2$ and $x_f \in [0.25, 0.33]$. (bottom left) $K = 0.72$, $\tau \in [0.2, 0.29]$ and $x_f = 0.25$. (bottom right) $K \in [0.72, 0.99]$, $\tau = 0.2$ and $x_f = 0.25$.

$f^+_{pj} = 2\gamma Ma \sin(j\pi x_p)\cos(\omega_f t)$. We seek the synchronisability for a range of parameters, each requiring us to obtain a new phase sensitivity function using the method described for our base case.

The synchronisability for varied x_p along the tube is shown in figure 5 for a wide range of parameters. In all cases, the maximum value of synchronisability occurs at $x_p = 0.5$, i.e., half way along the Rijke tube. The fact that the optimal location is at the tube mid-point could be attributed to the natural acoustic mode-shapes which all have a maximum at the midpoint. It also aligns with what was discovered for passive control via an adjoint analysis of the eigenvalue sensitivities (Magri & Juniper 2013) where a pressure based feedback forcing of the pressure equation was found to be maximal near the tube centre (around $x_p = 0.58$). The difference between their location and ours could be due to the choice of linearisation. Namely, the fact that ours is around the limit cycle whereas theirs is around a fixed point. This is an important consideration since Juniper (2011) shows that there are multiple stable limit cycles for a given set of parameters. As these come from the same fixed-point they will share the same eigenvalue-based conclusions. However, linearising about the limit cycle enables to form of the periodic orbit to influence the resulting adjoint solution and may lead to different conclusions.

Interestingly, in all cases the flame location induces an inflection point, with figure 5 (top) showing that this inflection moves with the flame location causing a new local maximum to occur to the left of the flame. While this may suggest that the flame locally inhibits synchronisation for pressure-based actuation, we should be careful in interpreting the behaviour at the flame due to the Galerkin method used to solve the equations. The Galerkin projection does not capture the jump

Rapids articles must not exceed this page length

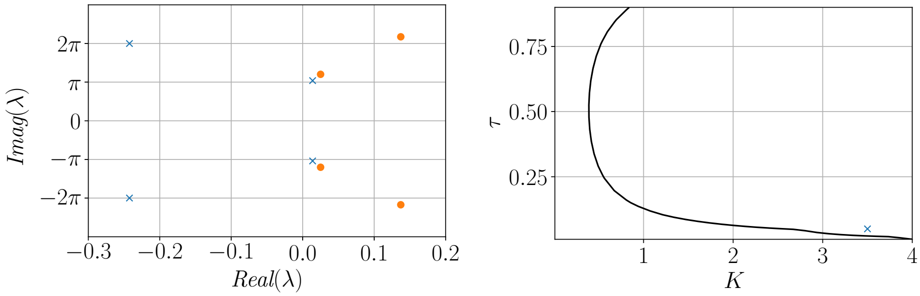

Figure 6: (left) Eigenvalues for the one frequency (blue crosses) and two frequency (orange circles) systems. (right) Neutral curve for $x_f = 0.2$.

conditions that should be present at the flame, which could be explicitly treated by using a higher fidelity numerical scheme (Sayadi *et al.* 2014). By comparing figures 5 (bottom left) and 5 (bottom right) we see that the synchronisation dynamics are more sensitive to the flame time delay than the flame strength with synchronisation becoming harder as these parameters are increased. We note that the increased sensitivity with respect to time-delay agrees with the work of Aguilar *et al.* (2017) who showed this variable also gives the largest sensitivity in their thermoacoustic system using an adjoint-based analysis of the eigenvalues.

Now that many aspects of the phase sensitivity analysis have been presented, we consider one more parameter regime. For the baseline case considered so far the steady state $(u, p) = (0, 0)$ has one pair of unstable eigenvalues around the primary pure-acoustic angular frequency of $\omega = \pi$ (shown in figure 6 (left)). This figure also shows stable eigenvalues at the first harmonic of this mode with an angular frequency around $\omega = 2\pi$. The result is a limit cycle that is primarily dominated by one frequency. In order to consider a limit cycle with two dominant frequencies we can consider the neutral curve presented in Sayadi *et al.* (2014). For the flame location $x_f = 0.2$, the neutral curve shown in figure 6 (right) is obtained. We can see that around a flame strength of $K \approx 3$ a 'kink' develops in the neutral curve. As discussed in Sayadi *et al.* (2014), this 'kink' occurs because the secondary eigenvalue with $\omega \approx 2\pi$ becomes more unstable than the fundamental mode. Therefore, to consider the effect of two frequencies we now consider the case of $x_f = 0.2$, $K = 3.5$ and $\tau = 0.05$ (shown in figure 7 (right) to be located near the 'kink'). We note that for the parameter regime of this two frequency case, Sayadi *et al.* (2014) show that the mode shapes from a Galerkin approach show less agreement with a high fidelity approach that properly discretises the discontinuity at the flame. Therefore, as in our parametric study showcased in figure 5, we proceed with caution when interpreting the results. For these parameters figure 7 (left) shows that now both the fundamental and first harmonic are unstable, with the first harmonic being more unstable than the fundamental mode. As in the baseline-case this instability saturates into a limit cycle (see figure 7 (left)), where the presence of a second frequency is evident in its 'loop'.

Figure 7 (right) shows the Arnold tongues for $1:2$, $1:1$, $2:1$ and $3:1$ synchronisation for the same forcing used to produce figure 4 (right). We see that $1:1$ phase locking is easier in this system than the baseline. The reason for this could be attributed to the fact that figure 5 (left) suggests that synchronisation becomes easier as the flame time delay is decreased. However, it is also evident

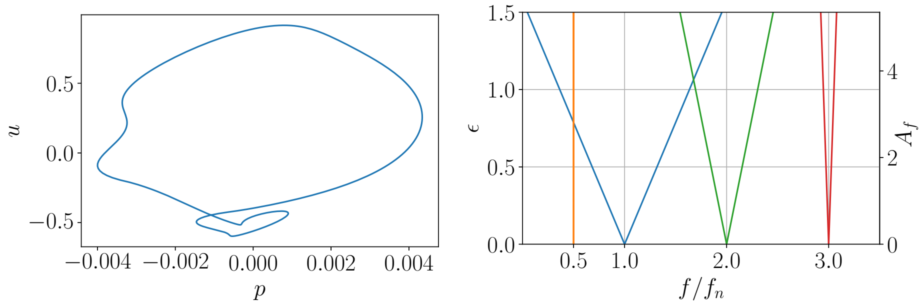

Figure 7: (left) Limit cycle for the multiple frequency system. (right) Arnold tongues for 1 : 2 (orange), 1 : 1 (blue), 2 : 1 (green) and 3 : 1 (red) synchronisation for our multiple frequency system.

that 2 : 1 phase locking is now more easily achievable than 3 : 1 phase locking which cannot be due to the smaller flame time delay alone. The reason for the increased 2 : 1 synchronisability for this double frequency case can be viewed as a direct consequence of having a more dominant first harmonic in the non-linear solution. This translates into an adjoint solution that contains more content at this frequency, which in turn leads to higher synchronisability via the phase coupling function.

We conclude our results by considering the potential speedups available over using fully non-simulations to find the Arnold tongues. For both methods a limit-cycle solution must first be found. Once this is found, we can estimate the subsequent cost of each analysis as follows. For both the phase sensitivity and fully non-linear methods the main cost involved is solving either the non-linear or adjoint equations, with any post processing, such as obtaining the phase coupling function, being negligible. If we assume that the non-linear and adjoint equations take the same amount of time t_{solve} to be solved, then the total time of the phase-sensitivity method is $C_{\text{p.s.}} = 2t_{\text{solve}}$. For the non-linear approach, if n_{f} frequencies and n_{A} amplitudes are used then the total time will be $C_{\text{n.l.}} = n_{\text{f}} n_{\text{A}} t_{\text{solve}}$. Therefore, the speedup using the phase-sensitivity approach is $Sp = C_{\text{n.l.}}/C_{\text{p.s.}} = n_{\text{f}} n_{\text{A}}/2$. For example, if $n_{\text{f}} = n_{\text{A}} = 10$ then the phase-sensitivity function approach will be around 50 times faster; a substantial speedup.

It is worth mentioning that the argument above does not take into account the fact that the non-linear approach will have only yielded the Arnold tongue for one particular forcing function and one choice of $n : m$ phase locking. If additional forcing functions or $n : m$ phase lockings are to be examined, then each case will call for another $C_{\text{n.l.}}$ time-units. However, the phase sensitivity function does not depend on the exact form of the forcing function or phase locking type considered, and therefore all subsequent analysis will be essentially free compared to the initial cost. These considerations further make the phase sensitivity function an efficient choice for determining the phase properties of a Floquet-stable system close to its limit cycle. Whilst adjoint approaches can be expensive in terms of memory, the fact that the phase sensitivity function is the adjoint neutral-Floquet mode means that it can be obtained using simulations over just one period of the limit cycle using an algorithm such as that presented by Barkley & Henderson (1996). Even though we do not take this approach here, utilising such a method could be critically important in rendering this analysis feasible for larger, memory-intensive systems.

6. Conclusion

We have performed phase reduction analysis to study the phase synchronisation properties of the thermoacoustic system in a Rijke tube with respect to the limit cycle produced by its instability. By reducing the phase dynamics to a scalar equation for the phase, we are able to reveal the effects of weak external forcing on the phase through the phase sensitivity function. The fact that this phase sensitivity function can be found through integration of the adjoint equation, and does not depend on the exact form of the external forcing, makes this analysis particularly efficient and generalisable. We utilised the phase description to map out the regions where $m : n$ phase locking can occur and identify the optimal positions along the Rijke tube where pressure actuation can result in synchronisation. The current study highlights the usefulness of phase sensitivity analysis for thermoacoustic problems, especially as an additional tool for designing open-loop control strategies via harmonic forcing.

Whilst keeping in mind that this method is not directly applicable to turbulent systems, unstable limit cycles, or for determining synchronisation behaviour far from a limit cycle, the present phase reduction analysis for a Rijke tube can be extended to suitable, more complex thermoacoustic simulations without major change. For future work, it would be interesting to first extend the analysis to a higher fidelity model of a Rijke tube (Sayadi *et al.* 2014) that explicitly treats the jump conditions at the flame, allowing for the phase dynamics near the flame, and for higher flame strengths, to be accurately quantified. Further to this, including the effects of a mean-flow in the Rijke tube model, and introducing velocity-based forcing, would also be beneficial in matching the synchronisation characteristics of some experimental setups. Applying phase techniques to more complex models including flame chemistry and more complex geometries would allow phase sensitivity analysis to play a role in the control of instabilities arising from more realistic combustion systems.

Acknowledgements. This work was supported by the US Air Force Office of Scientific Research (FA9550-16-1-0650, FA9550-21-1-0178; Program Managers: Douglas Smith and Gregg Abate).

Declaration of interests. The authors report no conflict of interest.

Data availability statement. The numerical code that supports the findings of this study is openly available at http://doi.org/10.5281/zenodo.4981470 (Skene & Taira 2021).

Author ORCID. C. S. Skene, https://orcid.org/0000-0003-0994-2013;
K. Taira, https://orcid.org/0000-0002-3762-8075

Appendix A. Mathematical details

For a DDE in the form (2.4) we see that the initial condition (initial history) must be specified over $-\tau \leqslant t \leqslant 0$ for the subsequent solution to be uniquely defined. In general, to propagate a state at time t_0 forward we need the solution to the DDE over $-\tau \leqslant t - t_0 \leqslant 0$. Therefore, it is helpful to think of the state as a function of the time-delay $\phi \in [-\tau, 0]$, i.e., for each time t we write a solution to the equation as $\boldsymbol{y}_t(\phi) = \boldsymbol{y}(t + \phi)$ (Hale 1977). In this manner, the solution to the DDE is a function and we can formally write $\boldsymbol{y}_t \in \mathcal{C}([-\tau, 0])$. An evolution equation can be found directly for the function $\boldsymbol{y}_t(\phi)$ and is defined piecewise as

$$\frac{\mathrm{d}\boldsymbol{y}_t(\phi)}{\mathrm{d}t} = \begin{cases} \frac{\mathrm{d}\boldsymbol{y}_t(\phi)}{\mathrm{d}\phi} & \text{if } \phi \in [-\tau, 0) \\ \boldsymbol{f}(t, \boldsymbol{y}_t(0)) + \boldsymbol{g}(t-\tau, \boldsymbol{y}_t(-\tau)) + \epsilon \boldsymbol{h}(t) & \text{if } \phi = 0 \end{cases}. \tag{A 1}$$

Similarly, the linearised equations (with $\epsilon = 0$) can be written as $\frac{\mathrm{d}\boldsymbol{y}_t(\phi)}{\mathrm{d}t} = \mathcal{A}\boldsymbol{y}_t(\phi)$ where the linear operator

$$\mathcal{A}\boldsymbol{y}_t(\phi) = \begin{cases} \frac{\mathrm{d}\boldsymbol{y}_t(\phi)}{\mathrm{d}\phi} & \text{if } \phi \in [-\tau, 0) \\ \boldsymbol{A}_1(t)\boldsymbol{y}_t(0) + \boldsymbol{A}_2(t)\boldsymbol{y}_t(-\tau) & \text{if } \phi = 0 \end{cases}. \tag{A 2}$$

As we are using an infinite dimensional description for solutions to our DDE, care is needed when defining the adjoint. For finite dimensional systems the adjoint is defined via an inner product since the direct and adjoint variables are defined in the same space, e.g., $\mathbb{R}^N$. However, for a DDE the direct variable $\boldsymbol{y}_t(\phi) \in \mathcal{C}([-\tau, 0])$, whereas the adjoint $\boldsymbol{y}_t^\dagger(\phi) \in \mathcal{C}([0, \tau])$. Hence, in order to define the adjoint, a bilinear form $V(\mathcal{C}([0,\tau]), \mathcal{C}([-\tau, 0])) \to \mathbb{R}$ is needed (see Wischert *et al.* (1994); Simmendinger *et al.* (1999); Kotani *et al.* (2012); Novičenko & Pyragas (2012)). In terms of our functional notation, the bilinear form (3.3) can be written as

$$\langle \boldsymbol{a}_t(\phi), \boldsymbol{b}_t(\phi)\rangle = \boldsymbol{a}_t(0)^T \boldsymbol{b}_t(0) + \int_{-\tau}^{0} \boldsymbol{a}_t(\phi+\tau)^T \boldsymbol{A}_2(t+\tau+\phi)\boldsymbol{b}_t(\phi)\,\mathrm{d}\phi. \tag{A 3}$$

The main steps of how to find the adjoint operator are now given and mainly follows the derivation available in Rand (2012).

To define the adjoint, we require that the bilinear form between a direct state and its adjoint (dual) state is constant in time (Simmendinger *et al.* 1999). Formally, this means that

$$\frac{\mathrm{d}}{\mathrm{d}t}\langle \boldsymbol{a}_t(\phi), \boldsymbol{b}_t(\phi)\rangle = 0. \tag{A 4}$$

Using definition (A 3), along with the fact that $\frac{\mathrm{d}\boldsymbol{y}_t(\phi)}{\mathrm{d}t} = \mathcal{A}\boldsymbol{y}_t(\phi)$ and the definition $-\frac{\mathrm{d}\boldsymbol{y}_t^\dagger(\phi)}{\mathrm{d}t} = \mathcal{A}^\dagger \boldsymbol{y}_t^\dagger(\phi)$, where $\mathcal{A}^\dagger$ is the yet to be found adjoint operator, we have

$$\begin{aligned} \frac{\mathrm{d}}{\mathrm{d}t}\langle \boldsymbol{a}_t(\phi), \boldsymbol{b}_t(\phi)\rangle =& \langle \boldsymbol{a}_t(\phi), \mathcal{A}\boldsymbol{b}_t(\phi)\rangle - \langle \mathcal{A}^\dagger \boldsymbol{a}_t(\phi), \boldsymbol{b}_t(\phi)\rangle \\ &+ \int_{-\tau}^{0} \boldsymbol{a}_t(\phi+\tau)^T \frac{\mathrm{d}\boldsymbol{A}_2(t+\tau+\phi)}{\mathrm{d}\phi}\boldsymbol{b}_t(\phi)\,\mathrm{d}\phi. \end{aligned} \tag{A 5}$$

We see that for no-time delay, setting this expression to zero gives the classic adjoint condition that $\langle \boldsymbol{a}_t(\phi), \mathcal{A}\boldsymbol{b}_t(\phi)\rangle = \langle \mathcal{A}^\dagger \boldsymbol{a}_t(\phi), \boldsymbol{b}_t(\phi)\rangle$. However, for a time-delayed system the infinite dimensional nature gives an extra term due to the memory of the system. Again using the inner product (A 3), we have that

$$\begin{aligned} \langle \boldsymbol{a}_t(\phi), \mathcal{A}\boldsymbol{b}_t(\phi)\rangle =& \boldsymbol{a}_t(0)^T \mathcal{A}\boldsymbol{b}_t(0) \\ &+ \int_{-\tau}^{0} \boldsymbol{a}_t(\phi+\tau)^T \boldsymbol{A}_2(t+\tau+\phi)\mathcal{A}\boldsymbol{b}_t(\phi)\,\mathrm{d}\phi, \end{aligned} \tag{A 6}$$

which upon using the definition of $\mathcal{A}$ (A 2) becomes

$$\begin{aligned}\langle \boldsymbol{a}_t(\phi), \mathcal{A}\boldsymbol{b}_t(\phi)\rangle =& \boldsymbol{a}_t(0)^T(\boldsymbol{A}_1(t)\boldsymbol{b}_t(0) + \boldsymbol{A}_2(t)\boldsymbol{b}_t(-\tau)) \\ &+ \underbrace{\int_{-\tau}^{0} \boldsymbol{a}_t(\phi+\tau)^T \boldsymbol{A}_2(t+\tau+\phi)\frac{\mathrm{d}\boldsymbol{b}_t(\phi)}{\mathrm{d}\phi}\,\mathrm{d}\phi}_{I}.\end{aligned} \tag{A 7}$$

The integral term I in (A 7) can be rearranged using integration by parts to give

$$\begin{aligned} I =& \left[\boldsymbol{a}_t(\phi+\tau)^T\boldsymbol{A}_2(t+\tau+\phi)\boldsymbol{b}_t(\phi)\right]_{-\tau}^{0} \\ &- \int_{-\tau}^{0}\left[\frac{\mathrm{d}\boldsymbol{a}_t(\phi+\tau)}{\mathrm{d}\phi}\right]^T \boldsymbol{A}_2(t+\tau+\phi)\boldsymbol{b}_t(\phi)\,\mathrm{d}\phi \\ &- \int_{-\tau}^{0} \boldsymbol{a}_t(\phi+\tau)^T\frac{\mathrm{d}\boldsymbol{A}_2(t+\tau+\phi)}{\mathrm{d}\phi}\boldsymbol{b}_t(\phi)\,\mathrm{d}\phi.\end{aligned} \tag{A 8}$$

Combining all the terms in (A 7) using the integral term in this form gives

$$\begin{aligned}\langle \boldsymbol{a}_t(\phi), \mathcal{A}\boldsymbol{b}_t(\phi)\rangle =& [\boldsymbol{A}_1(t)^T\boldsymbol{a}_t(0) + \boldsymbol{A}_2(t+\tau)\boldsymbol{a}_t(\tau)]^T\boldsymbol{b}_t(0) \\ &+ \int_{-\tau}^{0}\left[-\frac{\mathrm{d}\boldsymbol{a}_t(\phi+\tau)}{\mathrm{d}\phi}\right]^T \boldsymbol{A}_2(t+\tau+\phi)\boldsymbol{b}_t(\phi)\,\mathrm{d}\phi \\ &- \int_{-\tau}^{0} \boldsymbol{a}_t(\phi+\tau)^T\frac{\mathrm{d}\boldsymbol{A}_2(t+\tau+\phi)}{\mathrm{d}\phi}\boldsymbol{b}_t(\phi)\,\mathrm{d}\phi,\end{aligned} \tag{A 9}$$

which we recognise as

$$\begin{aligned}\langle \boldsymbol{a}_t(\phi), \mathcal{A}\boldsymbol{b}_t(\phi)\rangle =& \langle \mathcal{A}^\dagger\boldsymbol{a}_t(\phi), \boldsymbol{b}_t(\phi)\rangle \\ &- \int_{-\tau}^{0} \boldsymbol{a}_t^T(\phi+\tau)\frac{\mathrm{d}\boldsymbol{A}_2(t+\tau+\phi)}{\mathrm{d}\phi}\boldsymbol{b}_t(\phi)\,\mathrm{d}\phi,\end{aligned} \tag{A 10}$$

where the adjoint operator $\mathcal{A}^\dagger$ is now defined as

$$\mathcal{A}^\dagger\boldsymbol{y}_t^\dagger(\phi) = \begin{cases} -\frac{\mathrm{d}\boldsymbol{y}_t^\dagger(\phi)}{\mathrm{d}\phi} & \text{if } \phi\in(0,\tau] \\ \boldsymbol{A}_1^T(t)\boldsymbol{y}_t^\dagger(0) + \boldsymbol{A}_2^T(t+\tau)\boldsymbol{y}_t^\dagger(\tau) & \text{if } \phi = 0\end{cases}. \tag{A 11}$$

Substituting (A 10) into (A 5) then shows that the bilinear form between a direct state and its dual remains constant in time.

For a T-periodic system close to the limit cycle $\boldsymbol{y}_t^{\mathrm{LC}}(\phi)$, a state can be written as $\boldsymbol{y}_t(\phi) = \boldsymbol{y}_t^{\mathrm{LC}}(\phi) + \epsilon\boldsymbol{y}_t'(\phi)$. By the Floquet theorem (Floquet 1883), which carries over to delay differential equations (Simmendinger *et al.* 1999), the perturbation $\boldsymbol{y}_t'(\phi)$ can be written as

$$\boldsymbol{y}_t'(\phi) = \sum_i c_i \exp(\lambda_i t)\boldsymbol{y}_t^i(\phi), \tag{A 12}$$

where the Floquet modes $\boldsymbol{y}_t^i(\phi)$ are T-periodic functions, c_i are coefficients and $\lambda_i \in \mathbb{C}$ are the Floquet multipliers. This allows the idea of stability to be carried forward to periodic systems. If real$(\lambda_i) \leqslant 0$ for all i, then the limit cycle is stable and all perturbed states eventually return to the limit cycle (but generally with a phase shift), which is a necessary condition for our phase definition. For an autonomous system, there is always one neutral Floquet mode ($i = 0$) with $\lambda_0 = 0$. Moreover, the neutral mode shape can be found directly from the limit cycle solution via $\boldsymbol{y}_t^0(\phi) = \dot{\boldsymbol{y}}_t^{\mathrm{LC}}(\phi)$ (Simmendinger *et al.* 1999). It can be seen that this mode represents the phase shift since a Taylor expansion gives $\boldsymbol{y}_{t+\alpha}^{\mathrm{LC}}(\phi) \approx \boldsymbol{y}_t^{\mathrm{LC}} + \alpha\dot{\boldsymbol{y}}_t^{\mathrm{LC}}(\phi)$. Therefore, it is natural to use Floquet theory to understand the phase sensitivity function. We now demonstrate this using a similar approach to that of Novičenko & Pyragas (2012).

Consider the perturbed equation (2.4). Since the forcing term is small we can seek the solution in the form $\boldsymbol{y}_t(\phi) = \boldsymbol{y}_t^{\mathrm{LC}}(\phi) + \epsilon\boldsymbol{y}'_t(\phi)$. By linearising (2.4) we have that this perturbation is governed by the equation $\dot{\boldsymbol{y}}'_t(\phi) = \mathcal{A}\boldsymbol{y}'_t(\phi) + \mathcal{A}^h\boldsymbol{y}'_t(\phi)$ where

$$\mathcal{A}^h\boldsymbol{y}_t(\phi) = \begin{cases} 0 & \text{if } \phi \in [-\tau, 0) \\ h(t) & \text{if } \phi = 0 \end{cases}, \tag{A 13}$$

and $\mathcal{A}$ is defined as (A 2) from before. Now, since the perturbation is small and remains close to the limit cycle we can use the Floquet theorem to express the perturbation in the form

$$\boldsymbol{y}'_t(\phi) = \epsilon\sum_i c_i(t)\boldsymbol{y}_t^i(\phi). \tag{A 14}$$

From our previous discussion we know that only the $i = 0$ Floquet mode has the ability to change the phase of the system. Therefore, using a similar argument as before for each time t, the phase for the perturbed system must be $\theta = \omega_n t + \epsilon\omega_n c_0(t)$, giving its evolution equation as $\dot{\theta} = \omega_n + \epsilon\omega_n\dot{c}_0(t)$.

Now that we have found the phase equation in terms of the time-dependent coefficients of the Floquet-expansion, we can use the adjoint to relate $\dot{c}_0(t)$ to the forcing term $h(t)$. In order to do this, we first recognise that even though the Floquet modes are not orthogonal, the direct and adjoint Floquet modes form a bi-orthogonal set under our bilinear form (Simmendinger *et al.* 1999). In other words, with an appropriate normalisation of the adjoint, $\langle \boldsymbol{y}_t^{i,\dagger}(\phi), \boldsymbol{y}_t^j(\phi)\rangle = d_{i,j}\delta_{i,j}$ where $d_{i,j}$ are coefficients that depend on the normalisation and $\delta_{i,j}$ is the Kronecker delta. Note that for $i = j = 0$ this implies that $\langle \boldsymbol{y}_t^{0,\dagger}(\phi), \dot{\boldsymbol{y}}_t^{\mathrm{LC}}(\phi)\rangle = \omega_n$, where we have chosen the normalisation $d_{0,0} = \omega_n$. Using this biorthogonality, we can take the bilinear form of (A 14) with $\boldsymbol{y}_t^{0,\dagger}(\phi)$ to find $c_0(t)$ as $\langle \boldsymbol{y}_t^{0,\dagger}(\phi), \boldsymbol{y}'_t(\phi)\rangle = \epsilon\omega_n c_0(t)$. To find $\dot{c}_0(t)$, we differentiate this expression with respect to time. Using the already shown result that the time derivative of the contribution to this bilinear form from the unperturbed dynamics is zero, we obtain

$$\epsilon\omega_n\dot{c}_0(t) = \langle \boldsymbol{y}_t^{0,\dagger}(\phi), \mathcal{A}^h\boldsymbol{y}'_t(\phi)\rangle, \tag{A 15}$$

which, from the definition (A 13), becomes $\omega_n\dot{c}_0(t) = \boldsymbol{y}_t^{0,\dagger}(0)^T h(t)$. Hence, dropping the $i = 0$ superscript, the phase equation is (3.1) with $Z(\theta) = \boldsymbol{y}_{t=\theta/\omega_n}^{\dagger}(0)$.

REFERENCES

Aguilar, J. G., Magri, L. & Juniper, M. P. 2017 Adjoint-based sensitivity analysis of low-order thermoacoustic networks using a wave-based approach. *Journal of Computational Physics* **341**, 163–181.

Balasubramanian, K. & Sujith, R. I. 2008 Thermoacoustic instability in a rijke tube: Non-normality and nonlinearity. *Physics of Fluids* **20** (4), 044103.

Barkley, D. & Henderson, R. D. 1996 Three-dimensional floquet stability analysis of the wake of a circular cylinder. *Journal of Fluid Mechanics* **322**, 215–241.

Boccaletti, S., Pisarchik, A. N., del Genio, C. I. & Amann, A. 2018 *Synchronization: From Coupled Systems to Complex Networks*. Cambridge University Press.

Candel, S. 2002 Combustion dynamics and control: Progress and challenges. *Proceedings of the Combustion Institute* **29** (1), 1–28, proceedings of the Combustion Institute.

Correa, S. M. 1998 Power generation and aeropropulsion gas turbines: From combustion science to combustion technology. *Symposium (International) on Combustion* **27** (2), 1793–1807.

Culick, F. E. C. 1996 *Combustion Instabilities in Propulsion Systems*, *Nato Science Series E:*, vol. 306, pp. 173–241. Dordrecht: Springer.

Dowling, A. P. & Morgans, A. S. 2005 Feedback control of combustion oscillations. *Annual Review of Fluid Mechanics* **37** (1), 151–182.

Dupère, I. D. J. & Dowling, A. P. 2005 The Use of Helmholtz Resonators in a Practical Combustor. *Journal of Engineering for Gas Turbines and Power* **127** (2), 268–275.

Ermentrout, G. B. & Terman, D. 2010 *Mathematical Foundations of Neuroscience*, *Interdisciplinary Applied Mathematics*, vol. 35. New York, NY: Springer.

Floquet, G. 1883 Sur les équations différentielles linéaires à coefficients périodiques. *Annales scientifiques de l'École Normale Supérieure* **12**, 47–88.

Hale, J. K. 1977 *Theory of functional differential equations*, *Applied Mathematical Sciences*, vol. 3. New York, NY: Springer-Verlag.

Heckl, M. A. 1990 Non-linear acoustic effects in the rijke tube. *Acta Acustica united with Acustica* **72** (1), 63–71.

Iima, M. 2019 Jacobian-free algorithm to calculate the phase sensitivity function in the phase reduction theory and its applications to Kármán's vortex street. *Phys. Rev. E* **99**, 062203.

Juniper, M. P. 2011 Triggering in the horizontal rijke tube: non-normality, transient growth and bypass transition. *Journal of Fluid Mechanics* **667**, 272–308.

Juniper, M. P. & Sujith, R. I. 2018 Sensitivity and nonlinearity of thermoacoustic oscillations. *Annual Review of Fluid Mechanics* **50** (1), 661–689.

Kashinath, K., Li, L. K. B. & Juniper, M. P. 2018 Forced synchronization of periodic and aperiodic thermoacoustic oscillations: lock-in, bifurcations and open-loop control. *Journal of Fluid Mechanics* **838**, 690–714.

Kawamura, Y. & Nakao, H. 2015 Phase description of oscillatory convection with a spatially translational mode. *Physica D: Nonlinear Phenomena* **295-296**, 11–29.

Khodkar, M. A., Klamo, J. T. & Taira, K. 2021 Phase-locking of laminar wake to periodic vibrations of a circular cylinder. *Phys. Rev. Fluids* **6**, 034401.

Khodkar, M. A. & Taira, K. 2020 Phase-synchronization properties of laminar cylinder wake for periodic external forcings. *Journal of Fluid Mechanics* **904**, R1.

King, L. V. 1914 XII. On the convection of heat from small cylinders in a stream of fluid: Determination of the convection constants of small platinum wires with applications to hot-wire anemometry. *Philosophical Transactions of the Royal Society of London. Series A, Containing Papers of a Mathematical or Physical Character* **214** (509-522), 373–432.

Kotani, K., Yamaguchi, I., Ogawa, Y., Jimbo, Y., Nakao, H. & Ermentrout, G. B. 2012 Adjoint method provides phase response functions for delay-induced oscillations. *Phys. Rev. Lett.* **109**, 044101.

Kuramoto, Y. 1984 *Chemical Oscillations, Waves, and Turbulence*. Berlin: Springer-Verlag.

Lieuwen, T. C. & Yang, V. 2005 *Combustion Instabilities in Gas Turbine Engines: Operational Experience, Fundamental Mechanisms, and Modeling*, *Progress in astronautics and aeronautics*, vol. 210. Reston, VA: American Institute of Aeronautics and Astronautics.

Loe, I. A., Nakao, H., Jimbo, Y. & Kotani, K. 2021 Phase-reduction for synchronization of oscillating flow by perturbation on surrounding structure. *Journal of Fluid Mechanics* **911**, R2.

Magri, L. 2019 Adjoint Methods as Design Tools in Thermoacoustics. *Applied Mechanics Reviews* **71** (2).

Magri, L. & Juniper, M. P. 2013 Sensitivity analysis of a time-delayed thermo-acoustic system via an adjoint-based approach. *Journal of Fluid Mechanics* **719**, 183–202.

Mahashabde, A., Wolfe, P., Ashok, A., Dorbian, C., He, Q., Fan, A., Lukachko, S., Mozdzanowska, A., Wollersheim, C., Barrett, S. R. H., Locke, M. & Waitz, I. A. 2011 Assessing the environmental impacts of aircraft noise and emissions. *Progress in Aerospace Sciences* **47** (1), 15 – 52.

McManus, K. R., Poinsot, T. & Candel, S. M. 1993 A review of active control of combustion instabilities. *Progress in Energy and Combustion Science* **19** (1), 1–29.

Mondal, S., Pawar, S. A. & Sujith, R. I. 2019 Forced synchronization and asynchronous quenching of periodic oscillations in a thermoacoustic system. *Journal of Fluid Mechanics* **864**, 73–96.

Nair, A. G., Taira, K., Brunton, B. W. & Brunton, S. L. 2021 Phase-based control of periodic fluid flows. *Journal of Fluid Mechanics* **927**, A30.

Novičenko, V. & Pyragas, K. 2012 Phase reduction of weakly perturbed limit cycle oscillations in time-delay systems. *Physica D: Nonlinear Phenomena* **241** (12), 1090 – 1098.

Pikovsky, A., Rosenblum, M. G. & Kurths, J. 2003 *Synchronization: a universal concept in nonlinear sciences*. Cambridge University Press.

Rackauckas, C. & Nie, Q. 2017 Differentialequations.jl–a performant and feature-rich ecosystem for solving differential equations in julia. *Journal of Open Research Software* **5** (1).

Rand, R. 2012 *Differential-Delay Equations*, pp. 83–117. Berlin, Heidelberg: Springer Berlin Heidelberg.

Rayleigh, J. L. 1878 The Explanation of Certain Acoustical Phenomena. *Nature* **18**, 319–321.

Rijke, P. L. 1859 LXXI. Notice of a new method of causing a vibration of the air contained in a tube open at both ends. *The London, Edinburgh, and Dublin Philosophical Magazine and Journal of Science* **17** (116), 419–422.

Roy, A., Mondal, S., Pawar, S. A. & Sujith, R. I. 2020 On the mechanism of open-loop control of thermoacoustic instability in a laminar premixed combustor. *Journal of Fluid Mechanics* **884**, A2.

Sayadi, T., Le Chenadec, V., Schmid, P. J., Richecoeur, F. & Massot, M. 2014 Thermoacoustic instability – a dynamical system and time domain analysis. *Journal of Fluid Mechanics* **753**, 448–471.

Simmendinger, C., Wunderlin, A. & Pelster, A. 1999 Analytical approach for the floquet theory of delay differential equations. *Phys. Rev. E* **59**, 5344–5353.

Skene, C. S. & Taira, K. 2021 csskene/phase-reduction_rijke-tube: Initial release. https://doi.org/10.5281/zenodo.4981470.

Taira, K. & Nakao, H. 2018 Phase-response analysis of synchronization for periodic flows. *Journal of Fluid Mechanics* **846**, R2.

Verner, J. H. 2010 Numerically optimal Runge–Kutta pairs with interpolants. *Numerical Algorithms* **53** (2-3), 383–396.

Wischert, W., Wunderlin, A., Pelster, A., Olivier, M. & Groslambert, J. 1994 Delay-induced instabilities in nonlinear feedback systems. *Phys. Rev. E* **49**, 203–219.

Yang, D., Sogaro, F. M., Morgans, A. S. & Schmid, P. J. 2019 Optimising the acoustic damping of multiple helmholtz resonators attached to a thin annular duct. *Journal of Sound and Vibration* **444**, 69–84.

Zhao, D. & Li, X. Y. 2015 A review of acoustic dampers applied to combustion chambers in aerospace industry. *Progress in Aerospace Sciences* **74**, 114–130.

Zhao, D., Lu, Z., Zhao, H., Li, X.Y., Wang, B. & Liu, P. 2018 A review of active control approaches in stabilizing combustion systems in aerospace industry. *Progress in Aerospace Sciences* **97**, 35–60.